Polymers with Tailored Electronic Structure for High Capacity Lithium Battery Electrodes

By *Gao Liu**, *Shidi Xun*, *Nenad Vukmirovic*, *Xiangyun Song*, *Paul Olalde-Velasco*, *Honghe Zheng*, *Vince S. Battaglia*, *Linwang Wang*, and *Wanli Yang**

[*] Dr. G. Liu, Dr. S. Xun, X. Song, Dr. H. Zheng, Dr. V.S. Battaglia
Environmental Energy Technologies Division
Lawrence Berkeley National Laboratory, Berkeley, C 94720 (USA)
E-mail: (gliu@lbl.gov)

[*] Dr. W.L. Yang, P. Olalde-Velasco
Advanced Light Source
Lawrence Berkeley National Laboratory, Berkeley, C 94720 (USA)
E-mail: (wlyang@lbl.gov)

Dr. L.W. Wang, Dr. N. Vukmirovic
Computational Research Division
Lawrence Berkeley National Laboratory, Berkeley, C 94720 (USA)

Keywords: (Conductive polymer, X-ray spectroscopy, Density funcational theory, Lithium batteries, Binder)

Lithium-ion batteries have gained widespread use in consumer electronics due to their high energy density and low weight. However, for electric vehicle applications, further improvements in capacity and safety are highly challenging but necessary for lowering the cost and extending the driving distance. Materials with high lithium storage capacity, such as silicon and tin based alloys, have recently been extensively studied for their potential applications as Lithium battery anodes. But the large-volume change associated with lithiation and delithiation severely hinders the practical employments.[1-7] Despite the intensive efforts,[6-12] an effective low-cost solution to the volume-change problem remains elusive. Here, we developed a new conductive polymer through a combination of material synthesis, x-ray spectroscopy, density functional theory, and battery cell testing. Contrasting other polymer binders, the tailored electronic structure of the new polymer enables lithium doping under the battery environment. The polymer thus maintains both electric conductivity and

mechanical integrity during the battery operation. More importantly, this conductive polymer matrix is compatible with the lithium-ion slurry manufacturing process. A simple mixing of commercial Si particles with this binder forms a slurry, which can be coated into a porous electrode.[13-15] Our low-cost silicon/polymer composite anodes exhibit extraordinary cycling performance with about 2100 mAh g^{-1} for Si, and 1400 mAh g^{-1} for the entire electrode, after 650 cycles without any conductive additive. Through the cyclic optimization of synthesis, spectroscopy and simulation techniques, this work implements the conceptual idea of combining binder and conductive additive into one material, solving the volume change problem of high capacity battery electrodes.

Silicon has long been found to have the highest capacity among lithium-ion storage materials, with a theoretical capacity of 4200 mAh g^{-1} for full lithiation.[16] This is about ten times higher than that of the currently used graphite based anodes.[7, 16] The application, however, suffers the three times volume expansion from Si to $Li_{15}Si_4$ phase during the lithiation process.[5-7] The large volume change tends to disrupt the integrity of the composite electrode, leading to drastic capacity fade.[3-5] Tremendous efforts have been made to address the volume change issue, including controlled voltage,[6, 7, 17] nano structuring,[8, 9, 18] and applying adhesive binder.[10-12, 17, 19, 20] Among these efforts, nanosizing the Si particles is a promising route to achieve high capacity and acceptable cycle life.[8, 9, 21-23] However, there are significant challenges to make robust electronic connection to nano Si particles. One approach is to generate Si nanowires that are directly attached to the current collector to achieve high-capacity cycling. [8, 24, 25] The disadvantage is the fabrication complexity and thus the high manufacturing cost. Another approach is to generate structured carbon/nano-Si composites instead of using pure Si materials. Carbon structures provide a conductivity matrix while Si serves as the Li-ion storage material.[9, 11, 26-28]

In such conventional approaches for maintaining the electrical and mechanical integrity, there are three components in porous electrode designs (**Figure 1**a), i.e., nanometer size of Si,[8, 9, 23, 29] conductive additives,[21] and polymer binders.[12, 30, 31]. Typically, nanoparticle active materials require high volume of conductive additive, such as acetylene black (AB), to ensure high inter-particle electric conductivity.[21] The high volume of additive reduces the volumetric and gravimetric lithium-ion storage capacity. More seriously, because the conductive additive has no mechanical binding force, it tends to be pushed away from the Si particles by the volume expansion, leading to broken electric connections.[4, 32]

Alternatively, conductive binder holds the promise of dual functionality of both binder and conductive additive, thus truly solving the electric connectivity problem. However, all previous works have only showed limited performance.[13, 15] The technical challenge stems from the reducing enviroment when the Si anode is lithiated. For example, the typically used *p*-type polyaniline (PAN) conductive polymer will not stay *p*-doped below potential 1V (Li/Li^+), therefore losing electronic conductivity when used in the Si anode, which is operated between the potential range of 0.01V-1V (Li/Li^+).[33]

In order to solve the crucial problem on electric connectivity of the binder, we focus on developing polymer binders that could be cathodically (*n*-type) doped for high electronic conductivity under the reducing environment for anodes.[34] Our strategy for accomplishing the goal is to tailor the energy levels of the polymer conduction state, i.e., the lowest unoccupied molecular orbital (LUMO), so that the electrons could cathodically dope the polymer to achieve adequent electronic conductivity. Mechanically, it is also crucial that the polymer is intimately adhered to Si particle surface. Both electrical and mechanical integrity of the electrodes will then be maintained throughout the battery operation (Figure 1b).

The molecular structures of the developed polymers, PFFO and PFFOMB as depicted in Figure 1c, are based on polyfluorene (PF)-type polymers. Two key function groups, carbonyl C=O and methylbenzoic ester -PhCOOCH$_3$ (MB), were introduced for tailoring the LUMO electronic states and for improving the polymer adhesion respectively, as elaborated below.

In order to achieve a properly tailored electronic structure, we have extensively applied synchrotron based soft x-ray absorption spectroscopy (XAS) on a series of polymers to monitor the unoccupied conduction states.[35, 36] XAS provides a simple but direct probe of the excitations of core level electrons to the unoccupied states, i.e., the lowest-energy XAS peaks directly correspond to the LUMO states.[35, 36] **Figure 2**a shows the XAS data collected on three selected PF type polymers and the traditionally used *p*-type PAN. It is evident that the carbonyl groups in PFFO and PFFOMB generate a new LUMO state at 284.7eV in XAS (blue arrow), much lower than that of the PF (black arrow) and PAN (purple arrow). The additional MB units in PFFOMB does not change the low energy position of this LUMO. Therefore, the carbonyl is the key function group that lowers the LUMO energy level. For simplicity, we then focus on PFFO to discuss this unique electronic structure that defines the electrical conductivity under lithium battery environment.

Firstly, the XAS results are qualitatively consistent with *ab-initio* density functional theory (DFT) calculations utilizing National Energy Research Scientific Computing Center (NERSC) facility. The calculated absolute LUMO energy of PFFO is much lower than that of PAN (Figure 2b). The quantitative discrepancy between the theoretical and experimental values are due to the 0.8eV higher electrostatic potential in PAN and the XAS factors that are ignored in such theoretical estimations, e.g. difference on core-hole effect, and intrinsic LDA band energy errors.[35] The aforementioned calculation works quantitatively much better for the relative comparison between PF and PFFO (see supplemental Figure S1), since almost all the

carbon atoms are under the same chemical environment in these two polymers, except for the extra carbonyl group in PFFO. The calculation shows an energy difference of 0.7eV on LUMO levels, consistent with the 0.65 eV in XAS experiments, and evidently confirms that the 284.7eV lower LUMO states originates from the carbonyl group.

Secondly, we investigated the lithium binding energy in PFFO and PAN under DFT calculations. For PFFO, its atomic binding energy is 2.46 eV with the Li atom binding directly to the carbonyl group. For PAN, however, the highest lithium binding energy is only 1 eV with the lithium atom placed atop of the benzene ring. Our calculated lithium metal cohesive energy per lithium atom is 2.0 eV, consistent with the maximum of previous reports.[37, 38] We then get the Li+Si binding energy of 2.42 eV because it is 0.42 V higher than the lithium metal potential.[39] Therefore the quanlitative difference between PFFO and PAN on the lithium binding energy is obvious: Li+PFFO (2.46eV) ≥ Li+Si (2.42eV) or Li+Li (2.0eV) > Li+PAN (1eV). This sequence of the binding energies suggests that, due to the carbonyl group, the lithium will interact with PFFO before Si lithiation, which does not happen for PAN. In addition, the prioritized interaction in the PFFO matrix may assist with the formation of a stable SEI.

Thirdly, the electron charge transfer between lithium and the polymer molecule is indicated by the atomic orbital projections of the LUMO and LUMO+1 levels in Figure 2b. The isosurface plot in Figure 2c shows that the electron doping from lithium to PFFO is almost complete with distinct LUMO and LUMO+1. While for PAN, there is a strong lithium *s*- and PAN *p*- hybridization with limied charge transfer (Figure 2d). Therefore, an electron is almost completely donated to PFFO, once the lithium is bound to the carbonyl site of the polymer.

The improvement on the electronic conductivity through lithium doping is experimentally vefiried by the impedance measurements (Figure 2e).[34] Circular voltammetry (CV) tests on the pure PFFOMB polymer film under a mimic condition of anodes in lithium-ion environment indicate an initial cathodical doping at 1.25 V (Li/Li^+), and the second around 0.5 V (Li/Li^+) (see supplemental Figure S2). Both dopings improve the film electronic conductivity, which was increased by five times when doping potential changes from 1 to 0.01 V (Li/Li^+) (Figure 2e). This is a potential range that will fulfill the operation of Si based anode in the lithium-ion chemistry.

In addition to the carbonyl groups that tailor the electric property, MB units are introduced in PFFOMB to improve the chain flexibility of the polymer; therefore significantly strengthen the mechanical binding force (**Figure 3**a) without disturbing the tailored electronic state (Figure 2a). The adhesion tests of our Si/polymer electrode laminate show significantly higher adhesion force of PFFOMB than PFFO (Figure 3a). Further, the TEM images of the electrodes before and after 32 charge-discharge cycles show that the PFFOMB polymer indeed maintains the mechanical integrity of the electrodes throughout the battery operation (Figure 3c-f).

Figure 4 presents the performance of the PFFOMB/Si based anode that is cast with Si to polymer weight ratio of 2:1, contrasting other matrix. The electrodes based on PAN and polyvinylidine difluoride (PVDF) showed poor performance due to the insulating nature of the polymer matrix. The Si/AB/PVDF and Si/PFFO electrodes are characterized by high starting capacity but fast fading, due to the loss of electrical and mechanical integrity respectively. With the designed electrical and mechanical properties, PFFOMB achieved both intimate electric contact for electron conduction and mechanical integrity, resulting in high specific capacity and stable cycling performance, with 2100 mAh g^{-1} for Si (1400 mAh g^{-1}

and 0.42mAh cm^{-2} for the electrode) after 650 cycles (Figure 4b). This is so far the best performance reported for pure Si based composite electrode without any conductive additive.

Figure 4c displays the rate performance for the electrode. There is over 70% of capacity retention at C rate discharge with only 100 mV higher average discharge potential than that of the C/25 rate discharge. The 1C rate performance, 2050 mAh g^{-1} for Si and 1360 mAh g^{-1} for the electrode, is comparable with the specifically engineered high power anode (about 1200 mAh g^{-1} at 1C rate).[40] This remarkable performance again originates from the improved electric connectivity of the PFFOMB polymer through the tailored electronic structure, which reduces Ohmic drop of the electrode at high current density.

In summary, through a combination of advanced tools of material synthesis, spectroscopic analysis and theoretical simulations, we developed a new conductive binder for solving the long-standing volume change problem in high capacity materials. The integrated experimental and theoretical results show that the developed polymer features much improved electric conductiviy and robust mechanical binding force, which mantains electric connectivity and acommodates the Si volume change simutanuously. The composite electrodes based on Si particles and PFFOMB polymer, without any conductive additive, exhibit so far the best performance in several critical aspects for commercial applications, including high capacity, long-term cycling, low over potential between charge and discharge, and good rate performance. The application of such conductive binder is of low-cost, compatible with current lithium slurry manufacture, and not limited to Si anode system. Additionaly, the novel approach of this work provides a rare scientific showcase on developing new materials by tailoring the key electronic states through combined techniques.

Experimental

Sample Preparation: All the starting chemical materials including Si nanoparticles are commercially available from Sigma-Aldrich. The electrodes were made by dispersing a defined amount of Si nanoparticle in the conductive polymer chlorobenzene solution. Coin cells were prepared with the typical lithium metal as counter electrode. The slurry mixing, electrode casting, and cell fabrication can be found in the literature[31].

X-ray Spectroscopy and Theoretical Calculations: X-ray absorption spectroscopy was performed at beamline 8.0.1 of the Advanced Light Source (ALS). SEM and TEM were performed at National Center for Electron Microscopy (NCEM). The theoretical calculations were performed using density functional theory at National Energy Research Scientific Computing Center (NERSC).

See Supporting Information for details on material synthesis, electrode casting, cell characterization, adhesion test, TEM and SEM, spectroscopy and theoretical calculation methods.

Supporting Information

Supporting Information is available online from Wiley InterScience or from the author.

Acknowledgements

The material research was funded by the Assistant Secretary for Energy Efficiency, Office of Vehicle Technologies of the U.S. DOE under contract no. DE-AC03-76SF00098. TEM was performed at National Center for Electron Microscopy (NCEM). X-ray spectroscopy at the Advanced Light Sources (ALS) is supported by the Director, Office of Science, Office of Basic Energy Sciences, of the U.S. DOE under Contract No. DE-AC02-05CH11231. The

computation used the resources of National Energy Research Scientific Computing (NERSC) Center. All the facilities are located at Lawrence Berkeley National Laboratory.

[1] J. Y. Huang, L. Zhong, C. M. Wang, J. P. Sullivan, W. Xu, L. Q. Zhang, S. X. Mao, N. S. Hudak, X. H. Liu, A. Subramanian, H. Fan, L. Qi, A. Kushima, J. Li, *Science* **2010**, *330*, 1515.
[2] Y.-M. Chiang, *Science* **2010**, *330*, 1485.
[3] J. Christensen, J. Newman, *J. Solid State Electrochem.* **2006**, *10*, 293.
[4] S. Renganathan, G. Sikha, S. Santhanagopalan, R. E. White, *J. Electrochem. Soc.* **2010**, *157*, A155.
[5] J. H. Ryu, J. W. Kim, Y. E. Sung, S. M. Oh, *Electrochem. Solid-State Lett.* **2004**, *7*, A306.
[6] M. N. Obrovac, L. J. Krause, *J. Electrochem. Soc.* **2007**, *154*, A103.
[7] J. Li, J. R. Dahn, *J. Electrochem. Soc.* **2007**, *154*, A156.
[8] C. K. Chan, H. L. Peng, G. Liu, K. McIlwrath, X. F. Zhang, R. A. Huggins, Y. Cui, *Nat. Nano.* **2008**, *3*, 31.
[9] A. Magasinski, P. Dixon, B. Hertzberg, A. Kvit, J. Ayala, G. Yushin, *Nat. Mater.* **2010**, *9*, 353.
[10] W. R. Liu, M. H. Yang, H. C. Wu, S. M. Chiao, N. L. Wu, *Electrochem. Solid-State Lett.* **2005**, *8*, A100.
[11] N. S. Hochgatterer, M. R. Schweiger, S. Koller, P. R. Raimann, T. Wohrle, C. Wurm, M. Winter, *Electrochem. Solid-State Lett.* **2008**, *11*, A76.
[12] J. Li, D.-B. Le, P. P. Ferguson, J. R. Dahn, *Electrochim. Acta* **2010**, *55*, 2991.
[13] S. Y. Chew, Z. P. Guo, J. Z. Wang, J. Chen, P. Munroe, S. H. Ng, L. Zhao, H. K. Liu, *Electrochem. Commun.* **2007**, *9*, 941.
[14] Z. P. Guo, J. Z. Wang, H. K. Liu, S. X. Dou, *J. Power Sources* **2005**, *146*, 448.
[15] Y. Liu, T. Matsumura, N. Imanishi, A. Hirano, T. Ichikawa, Y. Takeda, *Electrochem. Solid-State Lett.* **2005**, *8*, A599.
[16] B. A. Boukamp, G. C. Lesh, R. A. Huggins, *J. Electrochem. Soc.* **1981**, *128*, 725.
[17] D. Mazouzi, B. Lestriez, L. Roue, D. Guyomard, *Electrochem. Solid-State Lett.* **2009**, *12*, A215.
[18] Y. Yao, M. T. McDowell, I. Ryu, H. Wu, N. Liu, L. Hu, W. D. Nix, Y. Cui, *Nano Lett.* **2011**, [Please fill info here?].
[19] A. Magasinski, B. Zdyrko, I. Kovalenko, B. Hertzberg, R. Burtovyy, C. F. Huebner, T. F. Fuller, I. Luzinov, G. Yushin, *ACS Appl. Mater. Interfaces* **2010**, *2*, 3004.
[20] S. Komaba, K. Shimomura, N. Yabuuchi, T. Ozeki, H. Yui, K. Konno, *J. Phys. Chem. C* **2011**, [Please fill info here?].
[21] B. Kang, G. Ceder, *Nature* **2009**, *458*, 190.
[22] S. D. Beattie, D. M. Manolescu, S. L. Blair, *J. Electrochem. Soc.* **2009**, *156*, A44.
[23] J. Graetz, C. C. Ahn, R. Yazami, B. Fultz, *Electrochem. Solid-State Lett.* **2003**, *6*, A194.
[24] L. F. Cui, R. Ruffo, C. K. Chan, H. L. Peng, Y. Cui, *Nano Lett.* **2009**, *9*, 491.
[25] R. Teki, M. K. Datta, R. Krishnan, T. C. Parker, T. M. Lu, P. N. Kumta, N. Koratkar, *Small* **2009**, *5*, 2236.
[26] H. Kim, J. Cho, *Nano Lett.* **2008**, *8*, 3688.
[27] A. Timmons, A. D. W. Todd, S. D. Mead, G. H. Carey, R. J. Sanderson, R. E. Mar, J. R. Dahn, *J. Electrochem. Soc.* **2007**, *154*, A865.

[28] Y. Liu, Z. Y. Wen, X. Y. Wang, X. L. Yang, A. Hirano, N. Imanishi, Y. Takeda, *J. Power Sources* **2009**, *189*, 480.
[29] H. Kim, M. Seo, M. H. Park, J. Cho, *Angew. Chem. Int. Ed.* **2010**, *49*, 2146.
[30] G. Liu, H. Zheng, S. Kim, Y. Deng, A. M. Minor, X. Song, V. S. Battaglia, *J. Electrochem. Soc.* 2008, *155*, A887.
[31] G. Liu, H. Zheng, A. S. Simens, A. M. Minor, X. Song, V. S. Battaglia, *J. Electrochem. Soc.* 2007, *154*, A1129.
[32] S. D. Beattie, D. Larcher, M. Morcrette, B. Simon, J. M. Tarascon, *J. Electrochem. Soc.* **2008**, *155*, A158.
[33] A. Ray, G. E. Asturias, D. L. Kershner, A. F. Richter, A. G. Macdiarmid, A. *J. Epstein, Synth. Met.* **1989**, *29*, E141.
[34] T. R. Jow, L. W. Shacklette, *J. Electrochem. Soc.* **1988**, *135*, 541.
[35] F. de Groot, A. Kotani, *Core Level Spectroscopy of Solids*, CRC Press Taylor & Francis Group, Boca Raton **2008**.
[36] J. Sthör, *NEXAFS Spectroscopy*, Springer, **1996**.
[37] K. Doll, N. M. Harrison, V. R. Saunders, *J. Phys. Condens. Matter* **1999**, *11*, 5007.
[38] J. Paier, M. Marsman, G. Kresse, *J. of Chem. Phys.* **2007**, *127*, 024103.
[39] W.-J. Zhang, *J. Power Sources* **2011**, *196*, 13.
[40] R. Krishnan, T.-M. Lu, N. Koratkar, *Nano Lett.* **2010**, *11*, 377.

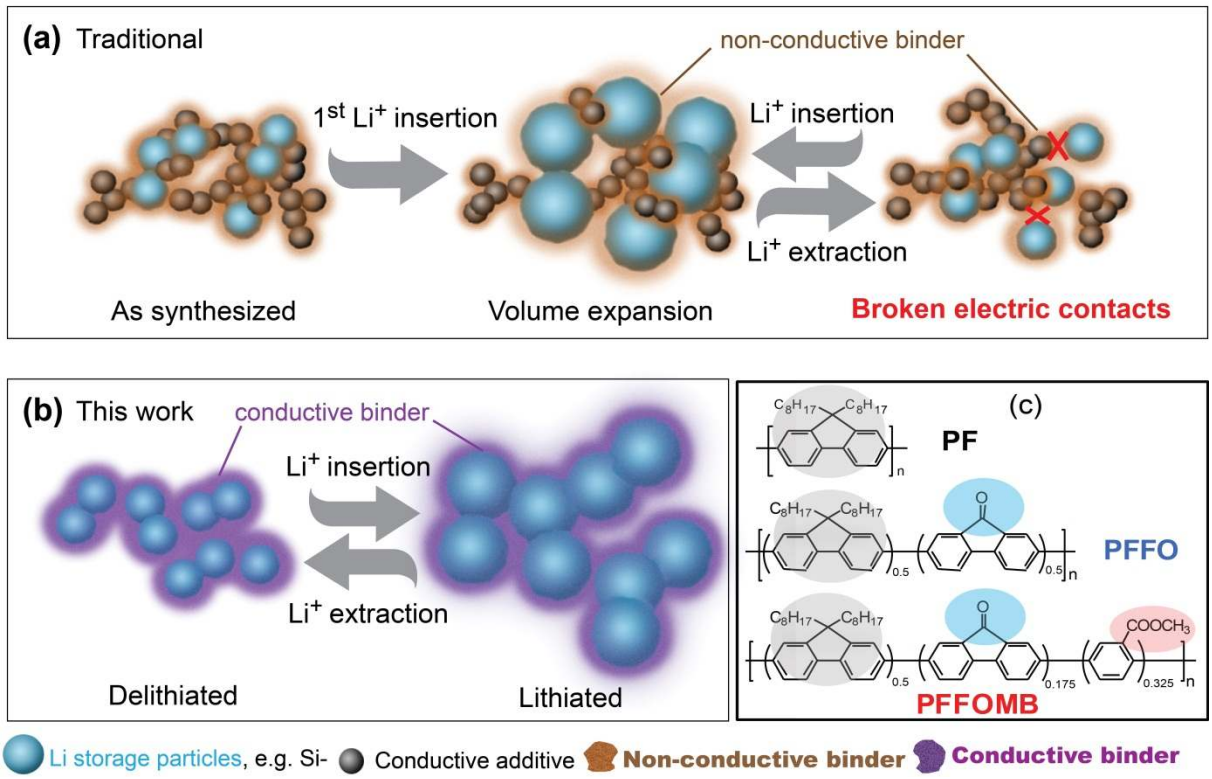

Figure 1. Schematics of the technical approaches to address volume change issue in battery materials. **(a)** Traditional approaches use acetylene black (AB) as the conductive additive and PVDF polymer as mechanical binder. **(b)** Conductive polymer with dual functionality, as a conductor and binder, could keep both electric and mechanical integrity of the electrode during the battery cycles. **(c)** The molecular structure of the PF-type conductive polymers, with two key function groups in PFFOMB, carbonyl and methylbenzoic ester, for tailoring the conduction band and for improving the mechanical binding force respectively.

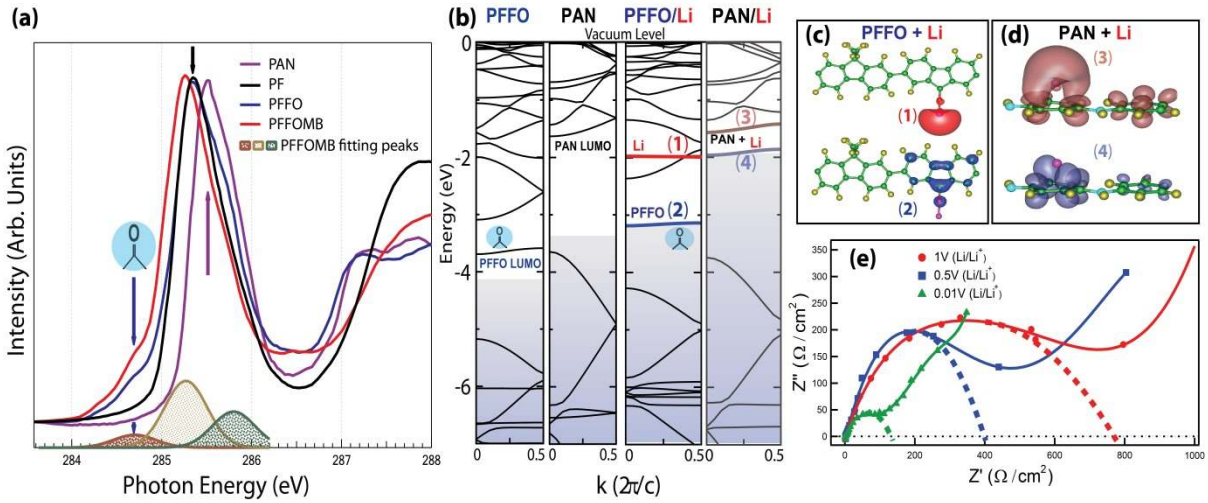

Figure 2. Tailored electronic structure and conductivity of the polymer. **(a)** Carbon-*1s* XAS spectra collected on a series of polymers. The three peaks at the bottom show the best peak fitting result of the spectrum of PFFOMB (see supplemental Figure S3). The carbonyl group leads to a much lower LUMO level at 284.7 eV (blue arrow). **(b)** Calculated band structure of PFFO (PFFO/Li) in comparison with PAN (PAN/Li). The k-point is along the polymer chain direction with *c* as the period length. Shaded area indicates occupied states. Fermi level floats between HOMO and LUMO for undoped materials. (1) and (4) are Li induced bands, which sits above (2), PFFO LUMO, but below (3), PAN LUMO. **(c-d)** The wavefunction square of the bands (1), (2), (3) and (4), as marked in (b). The isosurfaces encompass 50% of the wavefunction charge density. The distinct isosurfaces of bands (1) and (2) indicate that the electron charge transfer from Li to PFFO is almost complete, contrasting the weak charge transfer in PAN/Li with close isosurface shape of (3) and (4). **(e)** The enhanced conductivity of PFFOMB polymer (without Si) at different cathodical doping potentials. The dotted lines are extrapolations of the semi-circle lineshape. The interceptions of the dotted line with the horizontal zero-line indicate the film resistivity, which decreases from 770 to 120 Ω cm^{-2} when doping potential changes from 1 to 0.01 V (Li/Li^+).

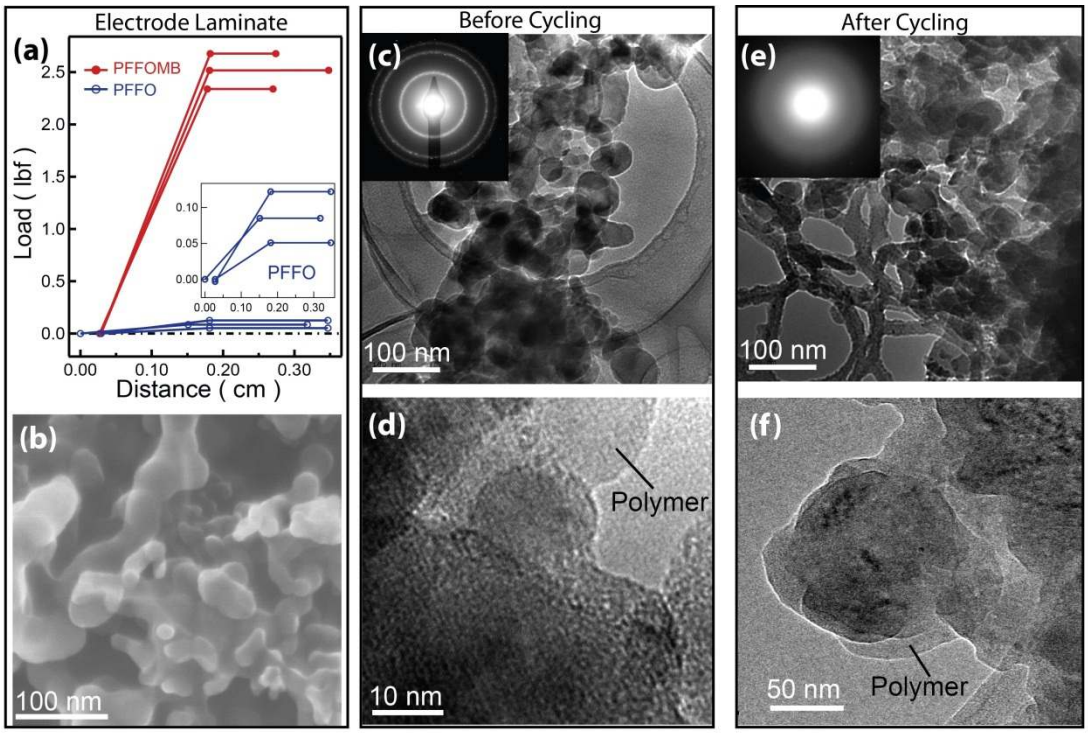

Figure 3. Physical properties of the Si/PFFOMB composite electrode. **(a)** Adhesion force plot of the Si/polymer electrode laminates. Insert is the amplified PFFO data. **(b)** SEM image of a standard porous microstructure of the surface of the Si/PFFOMB composite electrode. **(c-d)** TEM images of Si nanoparticles embedded in the as prepared PFFOMB polymer matrix. (Inset) electron diffraction pattern shows the crystalline nature of Si before cycling. **(e-f)** TEM images of Si nanoparticles maintained in the PFFOMB polymer matrix after 32 cycles. (Inset) electron diffraction pattern shows the loss of crystallinity of Si after cycling.

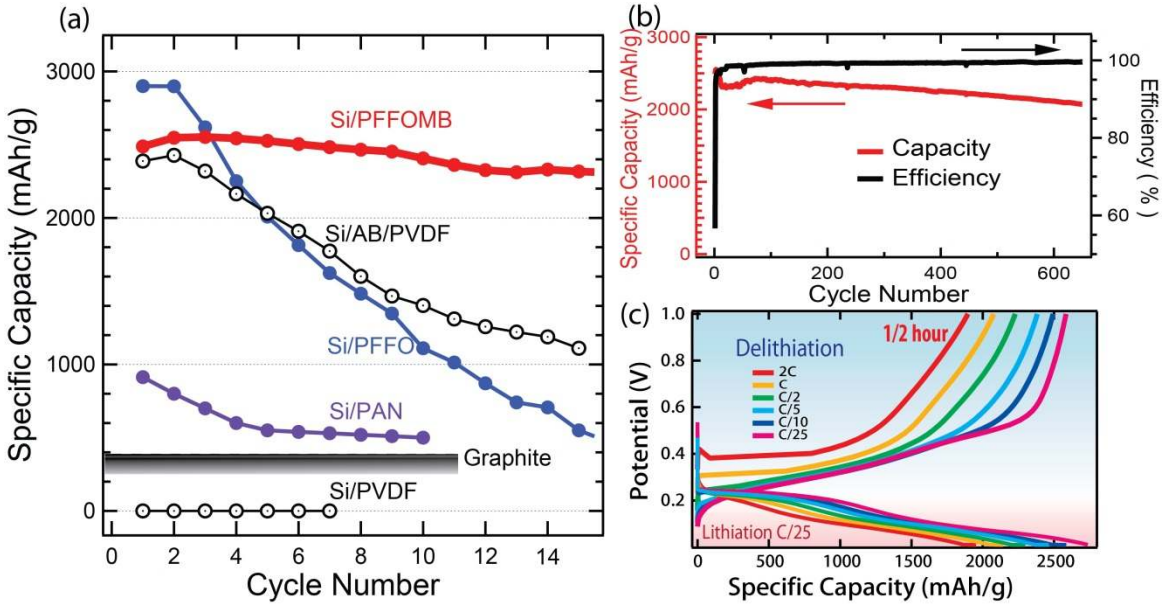

Figure 4. Cycling performance of Si/PFFOMB composite electrode. (a) The initial cycling behaviors of Si particles in different conductive matrixes against lithium metal counter electrodes at C/10 rate. (b) Cycling performance of Si/PFFOMB electrode between a cycling voltage of 1 V and 0.01 V for over 650 cycles at C/10 rate. (c) Electrode rate performance. C/n rate corresponds to discharging a cell in n hours. The top 6 curves show the delithiation rate at different C-rates. The bottom curves show lithiation at C/25 after the corresponding delithiation process.

The table of contents entry should be fifty to sixty words long, written in the present tense, and refer to the chosen figure.

A conductive polymer is developed for solving the volume change issue in lithium battery electrodes. Through combined techniques of synthesis, spectroscopy and simulation, the electronic structure of the polymer is tailored to enable *in-situ* lithium doping. Composite anodes based on this polymer and Si particles show remarkable Si cycling performance, with about 2100 mAh g^{-1} after 650 cycles without any conductive additive.

Keyword (Conductive polymer, X-ray spectroscopy, Density functional theory, Lithium batteries, Binder)

Gao Liu*, Shidi Xun, Nenad Vukmirovic, Xiangyun Song, Paul Olalde-Velasco, Honghe Zheng, Vince S. Battaglia, Linwang Wang, Wanli Yang*

Title (Polymers with Tailored Electronic Structure for High Capacity Lithium Battery Electrodes)

ToC figure

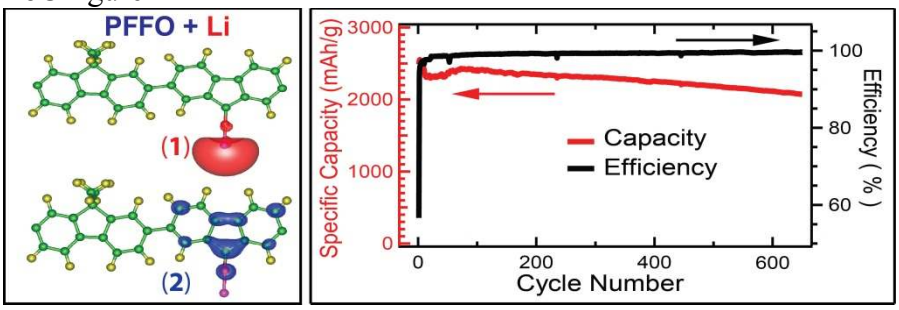

Supporting Information:

1. Materials and Methods

Raw Materials. All the starting chemical materials for synthesis the conductive polymer are purchase from Sigma-Aldrich. Battery-grade AB with an average particle size of 40 nm, a specific surface area of 60.4 $m^2 g^{-1}$, and a material density of 1.95 g cm^{-3} was acquired from Denka Singapore Private Ltd. PVDF KF1100 binder with a material density of 1.78 g cm^{-3} was supplied by Kureha, Japan. Anhydrous *N*-methylpyrrolidone NMP with 50 ppm of water content was purchased from Aldrich Chemical Co. Si nanoparticles were purchased from Sigma-Aldrich and used without further purification. The particle size defined by the company is less 100 nm. TEM analysis shows a bimodal particle size distribution at 50 nm and 10 nm diameter range. Lithium-ion electrolytes were purchased from Novolyte Technologies, including 1 M[is this Molar? if yes, all should be in small capitals!] $LiPF_6$ in ethylene carbonate (EC) and diethylene carbonate (DEC) (1:1 w/w) and 1 M $LiPF_6$ in EC and fluorinated ethylene carbonate (7:3 w/w).

Synthesis. PFFO, Poly(9,9-dioctylfluorene-co-fluorenone): A mixture of 9,9-dioctylfluorene-2,7-diboronic acid bis(1,3-propanediol) ester (0.826 g, 1.48 mmol), 2,7-dibromo-9-fluorenone (0.50 g, 1.48 mmol), $(PPh_3)_4Pd(0)$ (0.085 g, 0.074 mmol) and several drops of Aliquat 336 in a mixture of of toluene (10 mL), THF (2 mL) and 2 M Na_2CO_3 (5 mL) solution was refluxed with vigorous stirring for 72 h under an argon atmosphere. The copolymer was precipitated twice from a methanol/HCl mixture (ratio of 100/1, v/v). ^{1}H NMR (TMS, $CDCl_3$), δ (PPM): 8.10 (s, Ar-H), 7.88 (m, Ar-H), 7.64 (m, Ar-H), 2.10 (s, CH_2), 1.16 (m, CH_2), 0.80 (m, CH_2 and CH_3). GPC (THF, PS standard): *M*n = 3,200, *M*w/*M*n = 1.2.

Synthesis. PFFOMB, Poly(9,9-dioctylfluorene-co-fluorenone-co-methylbenzoic ester): A mixture of 9,9-dioctylfluorene-2,7-diboronic acid bis(1,3-propanediol) ester (0.80 g, 1.43 mmol), 2,7-dibromo-9-fluorenone (0.24 g, 0.72 mmol), methyl2,5-dibromobenzoate (0.21 g, 0.72 mmol), $(PPh_3)_4Pd(0)$ (0.082 g, 0.072 mmol) and several drops of Aliquat 336 in a mixture of of THF (13 mL) and 2 M Na_2CO_3 (5 mL) solution was refluxed with vigorous stirring for 72 h under an argon atmosphere. After reaction stopped, the solution was concentrated by vacuum evaporation and the polymer was precipitated from methanol. The resulting polymer was further purified by precipitating from methanol twice. The final polymer was collected by suction filtration and dried under vacuum with a yield of 87%. %. ^{1}H NMR (400 M Hz, $CDCl_3$) δ (ppm): 8.17 (s, Ar-H), 8.10 (s, Ar-H), 7.88 (m, Ar-H), 7.70 (m, Ar-H), 7.38-7.42 (d, Ar-H), 3.69 (s, OCH_3), 2.10 (br, CH_2), 1.2 (m, CH_2), 0.8-0.9 (m, CH_2, CH_3). Anal. Calcd. for $C_{19.95}H_{23}O_{0.71}$: C 87.40, H 8.46 Found: C 86.84, H 8.18. GPC (THF, PS standard): Mn = 36,000, PDI = 2.1.

Electrode Casting, Cell Fabrication and Testing. Si with conductive polymer mixtures was made by dispersing a defined amount of Si nanoparticle in the conductive polymer chlorobenzene solution to meet the desired Si to polymer weight ratios at 2:1. The slurry mixing, electrode casting, and cell fabrication can be found in the literature[1]. All the cell data reported are based on lithium metal as counter electrode in coin cells. The voltage rang is 0.01V-1V for the full capacity cycling. The C-rate calculation of the Si based electrode is assuming the Si has the theoretical capacity of 4200 mAh g^{-1}.

Electron Microscope. Composite electrode surface images were collected with Hitachi S-4300SE/N scanning electron microscopy (SEM) with an accelerating voltage of 15 kV using the high vacuum mode at room temperature. As also mentioned in Full Methods, high resolution transmission electron microscope (TEM) images were obtained on a Philips

CM200 field emission microscope operated at 200 kV at National Center for Electron Microscopy (NCEM) at LBNL.

Adhesion Test. Adhesion measurements of Si electrode were performed on a Chatillon® TCD225 series force measurement system. The Cu side of Si electrode (1 cm × 1 cm) was fixed vertically to the bottom sample holder. The adhesive side of a Scotch Magic® tape was firmly applied onto the electrode laminate side. The Scotch Magic® tape was peeled of using the top sample holder at the direction of 180° angle to the adhered tape and parallel to one side of the Si electrode, and at 10" min^{-1} moving rate to the bottom sample holder. A layer of the Si laminate was peeled off and adhered to the moving scotch magic tape. The force required to peel of the laminate was recorded as indication of the adhesion between the binder and Si materials. The first data point of each test, between 0 and 0.05 cm, corresponds to the beginning of the tape tension, with the forced offset to zero. When the tension is fully applied and the electrode laminate is peeled off, the measured force value reaches a plateau (2^{nd} and 3^{rd} data points in Fig.2b), representing the adhesion force of the electrode laminates.

Circular Voltammetry and Electro-impedance Spectroscopy. The CV were performed in an Ar-filled glove box. 27 μm of polymer film were coated on a 2.7 cm^2 stainless steel electrode. The potential sweep between 2 V and 0 V at 0.2 mV/s sweep rate. Lithium metal was used as counter and reference electrodes.
The conductivity of the film was measured with the film sandwiched in between two stainless steel electrodes. The sandwich film was brought to a certain potential before the impedance measurement was taken. The film conductivity was calculated based on the semi-circle of the impedance spectra. The electro-impedance spectroscopy measurement was performed at 0.01 Hz to 10^5 Hz range.

X-ray Absorption Spectroscopy. Carbon-*1s* XAS Spectra were collected at beamline 8.0.1 of the Advanced Light Source at LBNL. The undulator and spherical grating monochromator supply a linearly polarized photon beam with resolving power up to 6000[2]. Polymers were spin coated on clean Au surfaces then loaded into experimental chamber with base pressure of about 8×10^{-10}Torr. Experiments were done at room temperature and with the linear polarization of the incident beam 45^o to the sample surfaces. The XAS spectra shown here were collected in the total electron yield mode by registering the sample current normalized to the photon flux, which was measured simultaneously by the photocurrent of a clean Au mesh. All the samples have been measured multiple times with different flux and scan period, and data have been carefully checked to avoid effects from radiation damage. The overall resolution of the shown XAS spectra is better than 0.1 eV, and all the spectra plotted here were collected in one experiment to keep the relative shift of the LUMO level reliable.
Although the subjects on the XAS spectral lineshape are not within the scope of this manuscript, we would like to note that our spectral on *p*-type PAN is consistent with previous publications[3], and the low energy of the carbonyl induced band agrees well with the reported trend for such function group[4]. The results, however, are striking considering that the energy of the carbonyl induced $\pi^*_{C=O}$ transition in PF-type polymers is even lower than that of the $\pi^*_{C=C}$, which is typically the opposite in other polymers[5]. The same phenomena has been observed before in Fluorine substituted aromatic rings[6].

Theoretical Calculations. The calculations of electronic structure of the polymers and Li binding energies to the polymers were performed using density functional theory in local density approximation as implemented in the VASP code[7]. The projector augmented wave method[8] was used for the pseudopotentials. 400 eV plane wave cutoff was used and the atomic relaxation is stopped when the atomic forces are smaller than 10^{-2} eV $Å^{-1}$. In reality the

Li-polymer binding energy could be a little larger than the calculated value due to the possible sites for multiple co-binding for the lithium atom in a polymer blend.

Materials and Methods References

[1] G. Liu, H. Zheng, A. S. Simens, A. M. Minor, X. Song, V. S. Battaglia, *J. Electrochem. Soc.* **2007**, *154*, A1129.

[2] J. J. Jia, T. A. Callcott, J. Yurkas, A. W. Ellis, F. J. Himpsel, M. G. Samant, J. Stohr, D. L. Ederer, J. A. Carlisle, E. A. Hudson, L. J. Terminello, D. K. Shuh, R. C. C. Perera, *Rev. Sci. Instrum.* **1995**, *66*, 1394.

[3] M. Magnuson, J. H. Guo, S. M. Butorin, A. Agui, C. Sathe, J. Nordgren, A. P. Monkman, *J. Chem. Phys.* **1999**, *111*, 4756.

[4] S. G. Urquhart, H. Ade, The Journal of Physical Chemistry B 2002, 106, 8531.

[5] J. Sthör, *NEXAFS Spectroscopy*, Springer, **1996**.

[6] Y. Y. Luk, N. L. Abbott, J. N. Crain, F. J. Himpsel, *J. Chem. Phys.* **2004**, *120*, 10792.

[7] G. Kresse, J. Furthmuller, *Phys. Rev. B* **1996**, *54*, 11169.

[8] P. E. Blochl, *Phys. Rev. B* **1994**, *50*, 17953.

2. Supplementary Figures

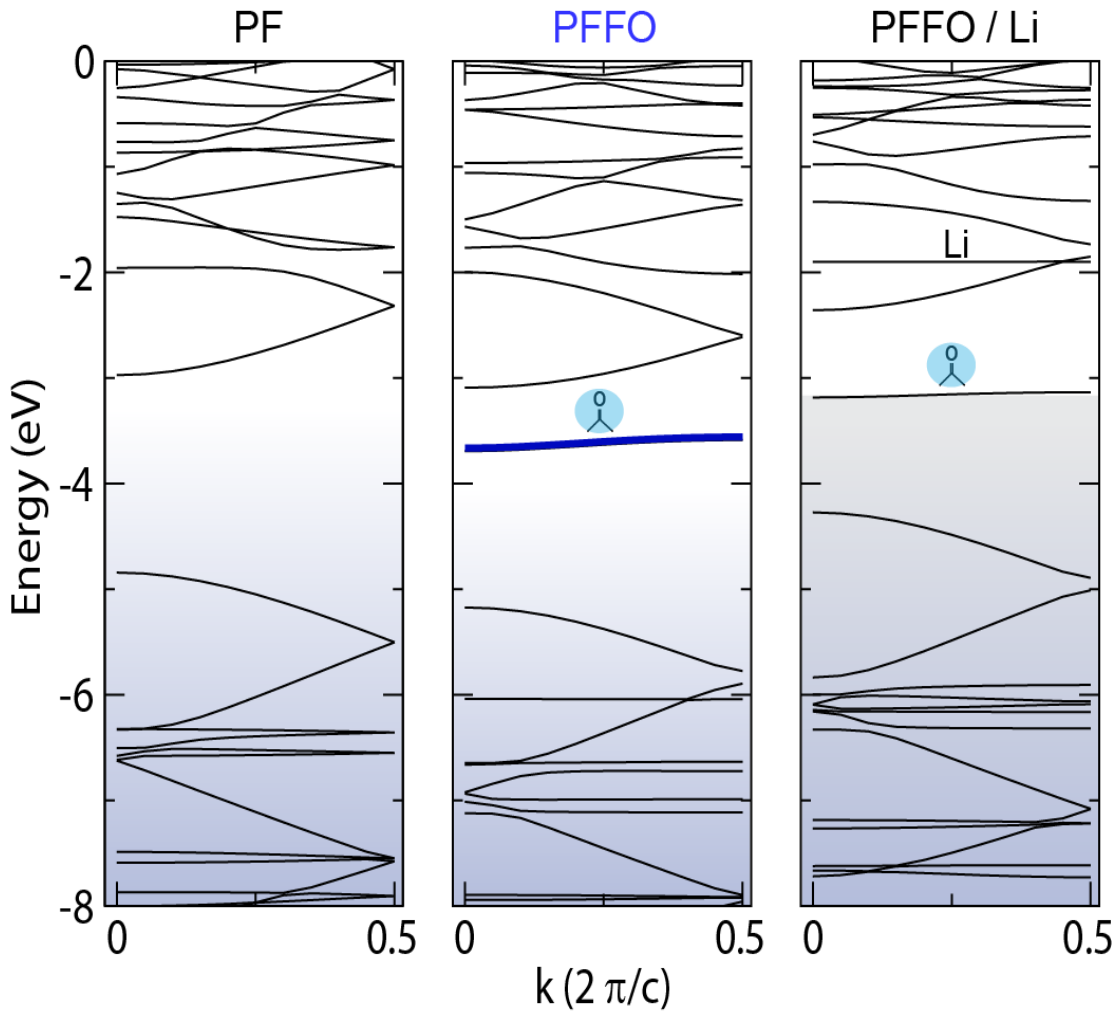

Figure S1: Band structure of PF, PFFO and PFFO with bound Li. The calculation methods and *k*-point definition are the same as those for Figure 2b. 0 eV energy is defined at the vacuum level. The comparison between the band structure of PF and PFFO evidently shows that introducing carbonyl group (C=O) leads to an additional low energy LUMO band (blue) for PFFO. This low energy LUMO is about 0.7 eV below the LUMO of PF, which is consistent with the 0.65 eV shift observed in XAS experiments (Figure 2a).

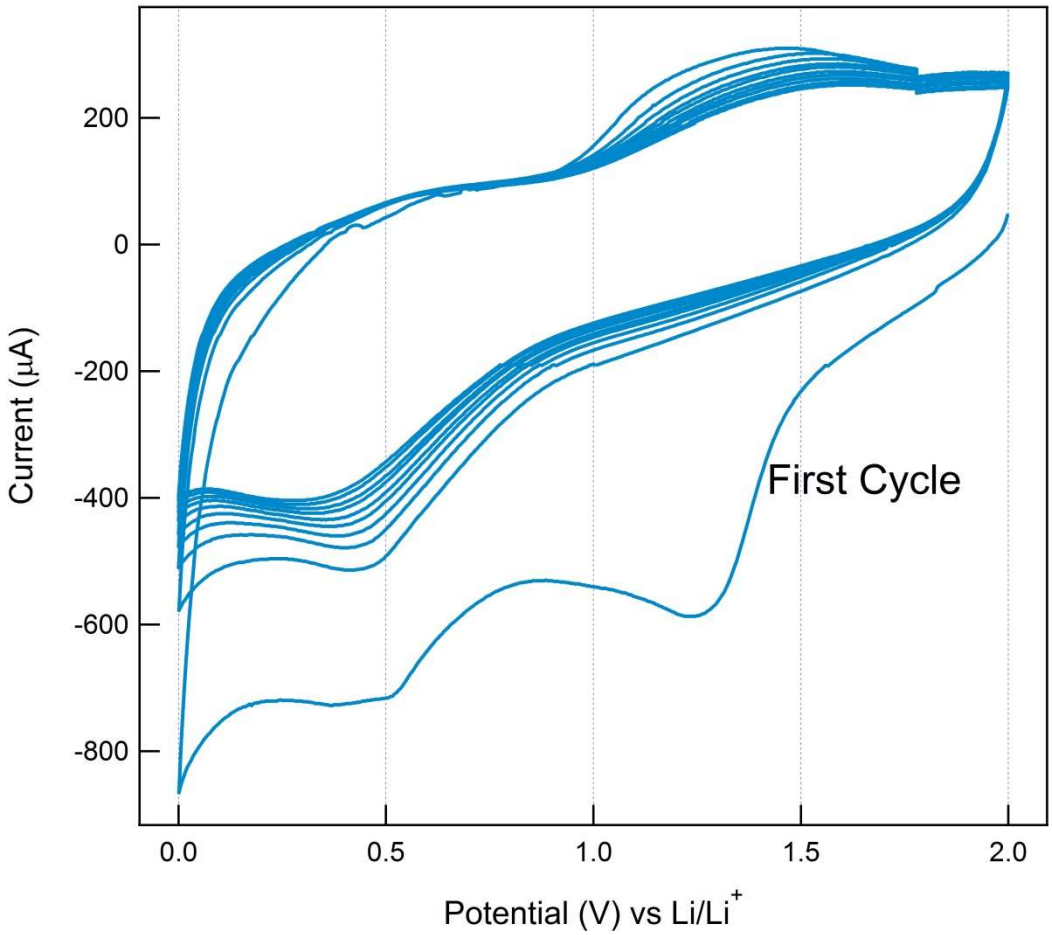

Figure S2: Circular Voltammogram of the PFFOMB (without Si) thin film in lithium-ion electrolyte. First cycle of lithium cathodical doping is different from rest of the cycles, indicating irreversible lithium ion bounding with the carbonyl groups. The CV curves show an initial cathodical doping at 1.25 V (Li/Li^+), and the second around 0.5 V (Li/Li^+).

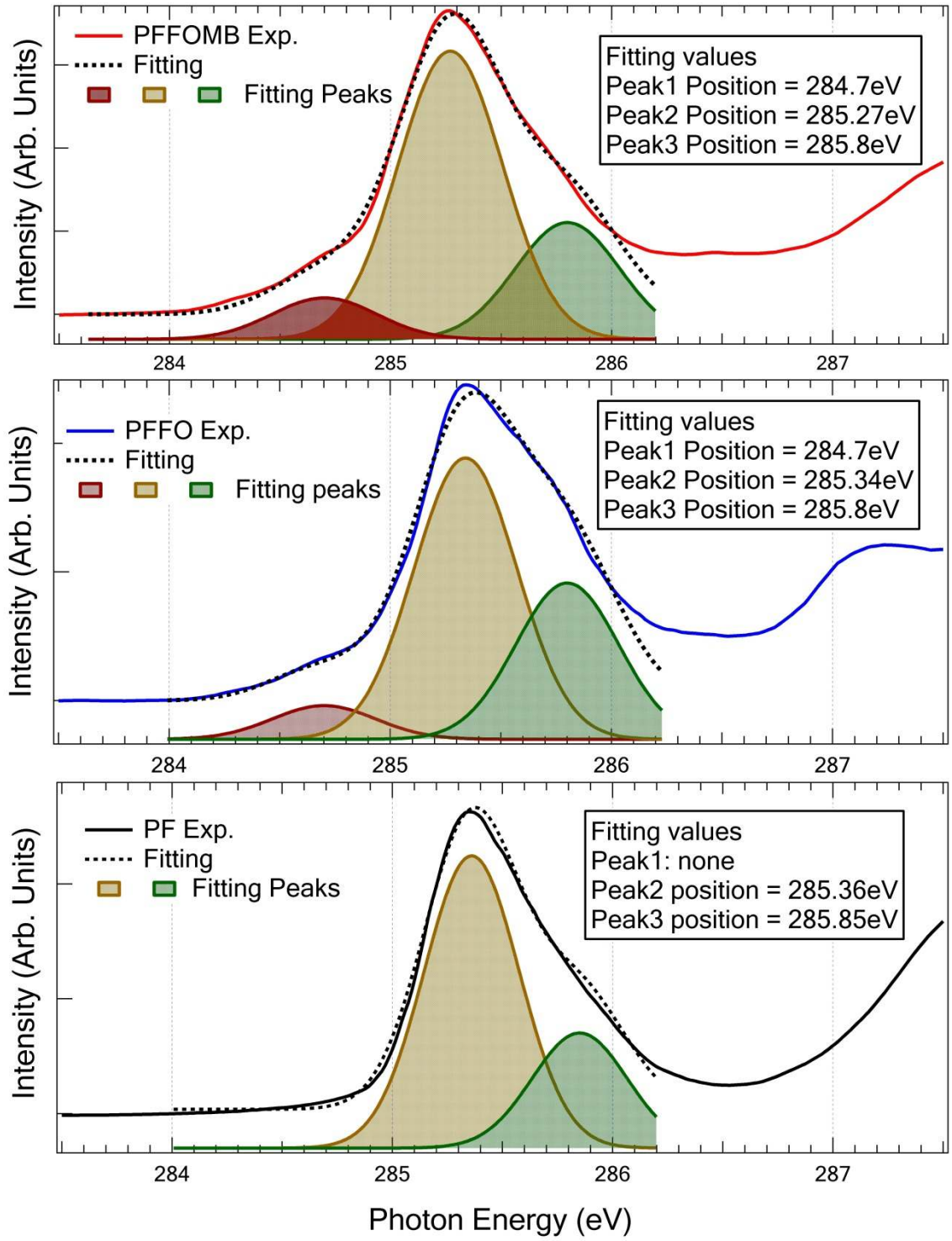

Figure S3: Gaussian peak fitting of the XAS spectra of PFFOMB, PFFO and PF. Dotted black lines are the best fitting with fitting peak positions listed in each panel. It clearly shows that the extra carbonyl C=O groups in PFFO and PFFOMB exhibit an extra peak at low energy of 284.7eV.